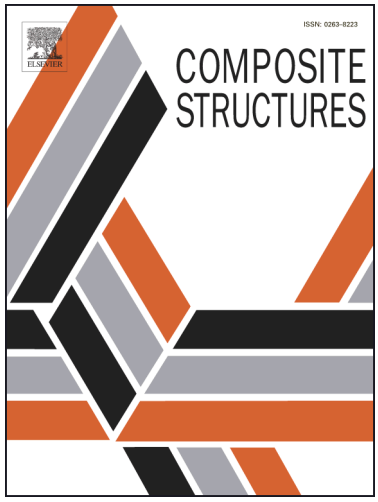

A novel implementation of asymptotic homogenization for viscoelastic composites with periodic microstructures

Quhao Li, Wenjiong Chen, Shutian Liu, Jiaxing Wang

PII: S0263-8223(17)33287-7
DOI: https://doi.org/10.1016/j.compstruct.2018.09.056
Reference: COST 10202

To appear in: *Composite Structures*

Received Date: 8 October 2017
Revised Date: 9 September 2018
Accepted Date: 18 September 2018

Please cite this article as: Li, Q., Chen, W., Liu, S., Wang, J., A novel implementation of asymptotic homogenization for viscoelastic composites with periodic microstructures, *Composite Structures* (2018), doi: https://doi.org/10.1016/j.compstruct.2018.09.056

A novel implementation of asymptotic homogenization for viscoelastic composites with periodic microstructures

Quhao Li[a,b], Wenjiong Chen[a], Shutian Liu[a,*], Jiaxing Wang[c]

[a] *State Key Laboratory of Structural Analysis for Industrial Equipment, Dalian University of Technology, Dalian, 116024, China*

[b] *School of Mechanical Engineering, Shandong University, Jinan 250061, PR China*

[c] *AVIC Shenyang Aircraft Design Research Institute, Shenyang 110035, China*

**Corresponding author. stliu@dlut.edu.cn*

Abstract：There is a growing demand for methods to estimate the effective viscoelastic response of viscoelastic composites, for their applications in structural vibration and noise control. This paper proposes a novel reformulation and numerical implementation algorithm for the asymptotic homogenization theory for predicting the effective complex moduli of viscoelastic composites in the frequency domain. In the new algorithm, an equivalent harmonic analysis is established and a double-layer elements method is proposed to solve the local problem in the homogenization process. On the basis of the new algorithm, the effective complex moduli can be obtained easily by using commercial software to serve as a black box. Numerous elements and techniques for modeling and analysis available in commercial software can be applied to complicated microstructures without mathematical derivation. The numerical examples presented show the validity of this new implementation algorithm.

Keywords: asymptotic homogenization; viscoelastic composites; complex moduli; loss factor; double-layer elements method

1 Introduction

Increasing demands for controlling vibration and noise in structures have boosted the search for high-performance wave or vibration-absorbing structures and materials. Active or semi-active vibration-control techniques (1-3) and the applications of passive damping (4) are two of the most widely used methods for effectively vibration absorption, over a range of frequencies. Of these methods, passive damping using viscoelastic materials is popular due to its simple implementation and cost-effectiveness. However, very few solid materials can reach the engineering standards necessary for damping applications. Viscoelastic composites, which have desirable damping

characteristics and provide design flexibility (5-7), have captured the attention of researchers (8-10). The increasing applications of the damping materials have also driven up demands for accurate estimation of the effective viscoelastic response of composites.

Micromechanical method provides overall behavior of the composites from known properties of their constituents through an analysis of a unit-cell model (11, 12), then the heterogeneous structure of the composite is replaced by a homogeneous medium with anisotropic properties. Several methods have been developed over the past few decades to theoretically predict the effective elastic properties of composite materials, such as self-consistent scheme (SCS) (13), generalized self-consistent scheme (GSCS) (14), the Mori–Tanaka method (M-T) (15), representative volume element method (RVE) (16) and asymptotic homogenization method (AH) (17). Of which, SCS, GSCS and M-T method are usually be applied to derive the approximate analytic formula of composite material with simple microstructures. When the geometry configuration of the microstructure is complex or material properties differ greatly between different phases, these methods often exhibit a large error. RVE method and AH method are two widely used numerical methods to determine the effective moduli of heterogeneous materials with complicated microstructures. These two methods all construct the boundary-value problems of the microstructure and then obtain the effective material properties of composite materials based on the characteristic displacement or strain fields. In RVE method, correct boundary conditions need to be applied to model different loading situations and the accuracy of the RVE approximation depends on how well the assumed boundary conditions reflect each of the myriad boundary conditions. Hori and Nemat-Nasser (18) presented a universal inequality which indicates that the homogeneous displacement and homogeneous traction boundary conditions will give the upper and lower bounds of the effective modulus, respectively. Asymptotic homogenization method, which is developed based on perturbation theory, can also be regarded as one particular RVE method with special boundary conditions when the first order perturbation expansion of displacement is considered only. Since microstructure is assumed to be periodic across the problem domain in AH method, periodic boundary conditions are applied. Unit strain field related forces are used to obtain the characteristic displacements and a special equivalent formulation is given for computing the effective elastic coefficients.

The effective viscoelastic performance of materials is characterized by the complex modulus $G = G^{'} + iG^{''}$, which is frequency-dependent (19). Both the real and imaginary parts are proportional to the storage energy and the dissipated energy in the materials, respectively. Hashin (20) gave the first explicit expressions for the complex moduli of composites reinforced by continuous elastic fibers and spherical particles by applying the correspondence principle to the

elastic concentric cylinder and the concentric sphere assemblage models, respectively. Christensen (21) derived analytical expressions for the upper and lower bounds of the effective complex shear modulus of a linear viscoelastic matrix containing either spherical voids or perfectly rigid spherical inclusions. Wang et al (22) extended the Eshelby-Mori-Tanaka method into the Laplace domain to examine the linearly viscoelastic behavior of a transversely isotropic material with aligned spheroidal inclusions and an isotropic material with randomly oriented inclusions. Luciano et al (23) studied the viscoelastic problem of composite materials with periodic microstructures, and obtained the formulas for the Laplace transform of the relaxation functions of the composite in terms of the properties of the matrix and the fibers as well as the function of the nine triple series. Tran et al (24) proposed a numerical multiscale method computing the response of structures made of linearly non-aging viscoelastic in the time domain based on RVE method. Yi etc. (25) systematically formulated a way of obtaining the effective viscoelastic moduli both in the time and frequency domain for viscoelastic composites with periodic microstructures by the asymptotic homogenization method. On basis of this method, Liu et al (26) predicted the viscoelastic properties of layered materials and obtained explicit formulas for predicting the viscoelastic relaxation modulus of layered materials. Recently, a two-step homogenization approach based on mechanics of structure genome (MSG) is proposed by Liu etc. (27) to predict the viscoelastic behaviors of textile composites. Microstructure designs for an optimal damping performance have been attempted by some scholars (28-32) by combining asymptotic homogenization techniques and the topology optimization method.

Due to its rigorous mathematical foundation, asymptotic homogenization has been one of the most widely used methods for predicting the effective coefficient of periodic composites (33-37). A few analytical solutions to the unit cell problems for laminated and particulate composites, such as grid-reinforced composite structures (38), have been derived by several asymptotic homogenization methods. However, for complicated microstructures, the numerical methods apply better due to the difficulty in obtaining analytical solutions. Contrary to the rapid development seen in commercial software for finite element analysis of macro-structural performance, development of tools for analyzing the microstructural performance is still important, although some commercial software or unified tools, such as Digimat (39, 40), Altair Multiscale Designer (41), SwiftComp (42) and Multimechanics (43), have been developed for determining the effective properties of composite materials based on different micromechanical methods, such as RVE, AH, MSG, etc. If the asymptotic homogenization process can be solved with existing commercial software without the need for any complicated mathematical derivation, and leveraging the powerful modeling and analytical techniques readily available in commercial software to obtain the effective moduli of

arbitrarily complicated microstructures, it would enhance the application of asymptotic homogenization methods in engineering or researches greatly. Motivated by this intention, Cheng et al (44) developed a novel implementation of the asymptotic homogenization method by using commercial finite element analysis（FEA）software in a black box role for predicting the effective elastic moduli of periodic materials. This new implementation method replaces generalized unit strains with equivalent characteristic displacement fields and can be implemented in commercial software with a unified code, without introducing any simplifying assumptions of the asymptotic homogenization method. In addition, this method has already been applied in calculating the effective elastic constant of periodic plate structures (45-47) and of periodic heterogeneous beams(48, 49). Zhang et al (50) extended this method to calculate the effective coefficient of thermal expansion of periodic composite materials. Zhao et al (51) applied this new method to predict the elastic properties of PVC/ABS/nano-$CaCO_3$ polymer nanocomposites.

Inspired by the work of Cheng et al (44), the work discussed in this paper proposes a novel reformulation and numerical implementation algorithm of the asymptotic homogenization theory for predicting the effective complex moduli of the periodic composites in the frequency domain for damping characteristics. Contrary to the elastic problem, the calculation of the asymptotic homogenization for the complex moduli of viscoelastic composites is categorized within the field of complex numbers. To solve this problem, an equivalent harmonic analysis is established and a double-layer elements method is proposed to solve the local problem in the homogenization process. The subroutine for solving the equivalent harmonic problem is available in commercial software. On the basis of the new algorithm, the effective complex moduli can be obtained easily by using commercial software in a black box role. Furthermore, inverse Fourier transformation can be applied to obtain the viscoelastic response in the time domain.

This paper is organized as follows: the asymptotic homogenization method for predicting the effective complex moduli of periodic composites and its finite-element formulation is introduced in Sections 2 and 3. The new reformulation and implementation of asymptotic homogenization on the basis of commercial software is proposed in Section 4. The flow chart of the method is included in Section 5. In Section 6, the method is applied to examples illustrating its effectiveness. Finally, the conclusions are drawn.

2 Asymptotic homogenization method for linear viscoelasticity in the frequency domain

The homogenization method has been developed from the studies of partial differential equations with rapid oscillating coefficients and has been applied to the estimate the effective

moduli of composites with periodic microstructures (33). In this section, a brief summary of the asymptotic homogenization method for obtaining the effective complex moduli is presented in order to render the paper self-contained, readers can see Ref. (17, 52) for the more details.

2.1 Governing equation for linear viscoelasticity

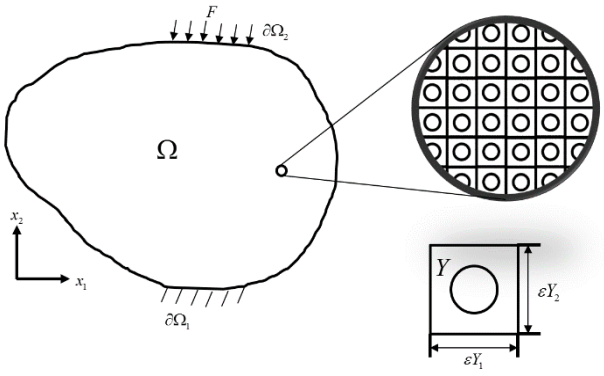

Fig. 1 Schematic representation of the periodic material and corresponding unit cell.

As shown in Fig. 1, Ω denotes a heterogeneous medium with periodic microstructures. It is assumed that the viscoelastic structure is under steady-state harmonic excitation with isothermal conditions. Applying the Correspondence Principle (53), the equation of motion for the structure at a fixed frequency ω is:

$$\frac{\partial \sigma_{ij}^{\varepsilon}(\boldsymbol{x})}{\partial x_j} = -\omega^2 \rho^{\varepsilon}(\boldsymbol{x}) u_i^{\varepsilon}(\boldsymbol{x}), \tag{1}$$

where ω is the excitation frequency; ρ^{ε} is the density of the material; $u_i^{\varepsilon}(\boldsymbol{x})$ and $\sigma_{ij}^{\varepsilon}(\boldsymbol{x})$ are the spatial parts of the displacement and stress, respectively. $\boldsymbol{x}$ denotes the position coordinate. ε represents the dependency of response fields on microstructural heterogeneities, i.e. response fields oscillate at the wavelengths of the order of characteristic volume size. Here and in the sequel, all Latin indexes assume 1,2,3 for 3D and 1,2 for 2D, and the repeated indexes are summed over the range. Bold fonts are reserved for tensor and matrix/vector representations. The constitutive response of the heterogeneous body is expressed as:

$$\sigma_{ij}^{\varepsilon}(\boldsymbol{x}) = G_{ijkl}(\omega)\varepsilon_{kl}^{\varepsilon}(\boldsymbol{x}), \tag{2}$$

where $\varepsilon_{kl}^{\varepsilon}(\boldsymbol{x})$ is the strain tensor and the $G_{ijkl}(\omega)$ is the complex modulus tensor, which is given by:

$$G_{ijkl}(\omega) = G'_{ijkl}(\omega) + iG''_{ijkl}(\omega), \tag{3}$$

where $i = \sqrt{-1}$, $G'_{ijkl}(\omega) \in R$ and $G''_{ijkl}(\omega) \in R$ denote the frequency-dependent storage modulus and loss modulus, respectively. Under the assumption of small deformation, the

relationship of strain-displacement can be written as:

$$\varepsilon_{ij}^{\varepsilon}(\boldsymbol{x}) = \frac{1}{2}\left(\frac{\partial u_j^{\varepsilon}(\boldsymbol{x})}{\partial x_i} + \frac{\partial u_i^{\varepsilon}(\boldsymbol{x})}{\partial x_j}\right), \tag{4}$$

Equations (1)-(3) are considered together with the following boundary conditions:

$$\begin{aligned} u_i^{\varepsilon}(\boldsymbol{x}) &= \bar{u}_i(\boldsymbol{x}); \qquad \boldsymbol{x} \in \partial\Omega_1, \\ \sigma_{ij}^{\varepsilon}(\boldsymbol{x}) n_j &= t_i(\boldsymbol{x}); \quad \boldsymbol{x} \in \partial\Omega_2, \end{aligned} \tag{5}$$

in which **n** is the outward unit normal vector along the traction boundaries. $\bar{u}_i(\boldsymbol{x})$ and $t_i(\boldsymbol{x})$ denote the prescribed displacement and traction data, respectively. For viscoelastic materials, the loss angle δ is defined by the ratio between the loss modulus (the imaginary part) and the storage modulus (the real part):

$$tan(\delta) = \frac{G''_{ijkl}(\omega)}{G'_{ijkl}(\omega)}. \tag{6}$$

This parameter measures the ability of a material to absorb energy and the relationship of (*ijkl*)-components between the loss modulus and the storage modulus can be written as:

$$G''_{ijkl}(\omega) = \eta_{ijkl}(\omega) G'_{ijkl}(\omega). \tag{7}$$

2.2 Asymptotic homogenization method in viscoelasticity

For the effective dynamic response of a periodic composite materials, there are two natural length scales in the problem, which are the microscale q that defines the fluctuations on the scale of microstructure Y and the macroscale $1/k_0$, where $k_0 = \omega/c_0$ is the wavenumber of the host medium, and c_0 is the wave velocity (54, 55). On the basis of these definitions, two independent length scales are introduced in the asymptotic homogenization method:

$$y_i = \frac{x_i}{L(\varepsilon)}, \ i = 1,2,3, \tag{8}$$

where $L(\varepsilon)$ is some expansion in ε, tending to zero as $\varepsilon \to 0$; $\varepsilon = qk_0 \ll 1$ is the small parameter denoting the relationship between the microscale q and macroscale $1/k_0$, so that x_i and y_i are short and long length scales, respectively. Let us suppose that we can expand the $L(\varepsilon)$ in asymptotic expansions of the form:

$$L(\varepsilon) = \varepsilon + L_2\varepsilon^2 + L_3\varepsilon^3 + O(\varepsilon^4). \tag{9}$$

Since the higher order dispersive corrections are not considered in this paper and equation (9) is simplified as $L(\varepsilon) = \varepsilon$. As a consequence of introducing the variable y_i, the derivatives must be transformed according to

$$\frac{\partial}{\partial x_i} \to \frac{\partial}{\partial x_i} + \frac{1}{\varepsilon}\frac{\partial}{\partial y_i}. \tag{10}$$

The most important and essential postulate in the homogenization method is that the field

variables are represented by asymptotic expansions in the following form:

$$\boldsymbol{u}^{\varepsilon}(\boldsymbol{x},\boldsymbol{y}) = \boldsymbol{u}^{(0)}(\boldsymbol{x},\boldsymbol{y}) + \varepsilon\boldsymbol{u}^{(1)}(\boldsymbol{x},\boldsymbol{y}) + \varepsilon^2\boldsymbol{u}^{(2)}(\boldsymbol{x},\boldsymbol{y}) + O(\varepsilon^3), \tag{11}$$

$$\sigma_{ij}^{\varepsilon}(\boldsymbol{x},\boldsymbol{y}) = \sigma_{ij}^{(0)}(\boldsymbol{x},\boldsymbol{y}) + \varepsilon\sigma_{ij}^{(1)}(\boldsymbol{x},\boldsymbol{y}) + \varepsilon^2\sigma_{ij}^{(2)}(\boldsymbol{x},\boldsymbol{y}) + O(\varepsilon^3). \tag{12}$$

It should be noted that $\boldsymbol{u}^{(m)}(\boldsymbol{x},\boldsymbol{y})$ is *Y*-periodic and independent of ε. By substituting equations (8), (10), (4) and (2) into equation (1) and considering the periodicity, one can readily eliminate the variable **y** from the first term $\boldsymbol{u}^{(0)}$, that is the leading order displacement $\boldsymbol{u}^{(0)}$ is a function of variable **x** only. Subsequently, by substituting equations (11), (12) and (10) into equation (1) and considering terms with like powers of ε, one obtains a series of differential equations of which the first two expressions are

$$\frac{\partial\sigma_{ij}^{(0)}}{\partial y_j} = 0, \tag{13}$$

$$\frac{\partial\sigma_{ij}^{(1)}}{\partial y_j} + \frac{\partial\sigma_{ij}^{(0)}}{\partial x_j} = -\omega^2\rho^{\varepsilon}(\boldsymbol{y})u_i^0(\boldsymbol{x}), \tag{14}$$

where

$$\sigma_{ij}^{(0)} = G_{ijkl}\left(\frac{\partial u_k^{(0)}}{\partial x_l} + \frac{\partial u_k^{(1)}}{\partial y_l}\right), \tag{15}$$

$$\sigma_{ij}^{(1)} = G_{ijkl}\left(\frac{\partial u_k^{(1)}}{\partial x_l} + \frac{\partial u_k^{(2)}}{\partial y_l}\right), \tag{16}$$

A combination of equations (13) and (15) leads to the following expression:

$$\frac{\partial}{\partial y_j}\left(G_{ijkl}\frac{\partial u_k^{(1)}(\boldsymbol{x},\boldsymbol{y})}{\partial y_l}\right) = -\frac{\partial G_{ijkl}(\boldsymbol{y})}{\partial y_j}\frac{\partial u_k^{(0)}(\boldsymbol{x})}{\partial x_l}, \tag{17}$$

which is defined over the unit cell. Taking advantage of the linearity of equation (17) and using the separation of variables, the displacement $\boldsymbol{u}^{(1)}(\boldsymbol{x},\boldsymbol{y})$ can be expressed as:

$$u_m^{(1)}(\boldsymbol{x},\boldsymbol{y}) = -\frac{\partial u_k^{(0)}(\boldsymbol{x})}{\partial x_l}\chi_m^{kl} + V_m(\boldsymbol{x}), \tag{18}$$

where χ_m^{kl} is the characteristic displacement. χ_m^{kl} is a 3rd rank tensor with symmetry on the second and third indices (i.e. $\chi_m^{kl} = \chi_m^{lk}$) and are periodic in **y**, which satisfies

$$\frac{\partial}{\partial y_j}\left(G_{ijmn}(\omega,\boldsymbol{y})\frac{\partial\chi_m^{kl}}{\partial y_n}\right) = \frac{\partial G_{ijkl}(\omega,\boldsymbol{y})}{\partial y_j}. \tag{19}$$

$V_m(\boldsymbol{x})$ is the homogenous solution of equation (17). It should be noted that equation (19) only depends on variable $\boldsymbol{y}$ and thus is solved within the domain of the unit cell, and this is referred to the unit cell problem or the local problem. χ_m^{kl} is normalized to ensure uniqueness:

$$\langle\chi_m^{kl}(\boldsymbol{y})\rangle = \frac{1}{|Y|}\int_Y \chi_m^{kl}(\boldsymbol{y})d\boldsymbol{y} = 0, \tag{20}$$

in which $\langle\bullet\rangle = \frac{1}{|Y|}\int_Y \bullet\, d\boldsymbol{y}$denotes the averaging operator in the unit cell, and $|Y|$ is the volume of

the unit cell. Substituting equations (18) and (15) into equation (14) and applying this averaging operator, exploiting the local periodicity of $\sigma^{(1)}$, we derive the homogenized equation of motion as:

$$G_{ijkl}^{H}\frac{\partial^2 u_k^{(0)}(\boldsymbol{x})}{\partial x_j \partial x_l} = -\omega^2 \rho_0 u_i^0(\boldsymbol{x}); \tag{21}$$

where the coefficients G_{ijkl}^{H} is the effective homogenized viscoelastic complex modulus which can be computed by:

$$G_{ijkl}^{H}(\omega) = \frac{1}{|Y|}\int_Y (G_{ijkl}(\omega,\boldsymbol{y}) - G_{ijmn}(\omega,\boldsymbol{y})\frac{\partial \chi_m^{kl}}{\partial y_m})\, d\boldsymbol{y}. \tag{22}$$

It can be noticed that equations (19) and (22) share the same formulations with the elastic homogenization method but in a complex number field. The following homogenized stress-strain relations can be obtained:

$$\tilde{\sigma}_{ij} = G_{ijkl}^{H}(\omega)\tilde{\varepsilon}_{kl}, \tag{23}$$

where $\tilde{\varepsilon}_{ij}$ and $\tilde{\sigma}_{ij}$ are the strain and stress tensor of the homogenized structure respectively. By now, we have derived the asymptotic homogenization method for obtaining the effective complex moduli of viscoelastic material. The procedure is summarized as:

Step 1: Solving the unit cell problem or the local problem (19) to obtain the characteristic displacements χ_m^{kl}.

Step 2: Computing the effective complex moduli $G_{ijkl}^{H}(\omega)$ by integrating over the domain of the unit cell based on the equation (22).

3 Finite element formulation

Analytical solutions to the unit cell problems for laminated, fiber-reinforced, and particulate composites have been already derived by researchers. However, for complicated microstructures, obtaining analytical solutions can be challenging and finite-element method is widely used to solve these problems. Integrating equation (19) over the domain **Y** and using the Gauss theorem with the consideration of the local periodicity boundary condition, the weak form of equation (19) can be written as:

$$\int_Y (G_{ijkl}(\omega,\boldsymbol{y}) - G_{ijmn}(\omega,\boldsymbol{y})\frac{\partial \chi_m^{kl}}{\partial y_n})\frac{\partial \overline{\chi}}{\partial y_j} d\boldsymbol{y} = 0, \quad \forall v_i \in V_y, \tag{24}$$

where $V_y = \{u_y(\boldsymbol{y}) \big| \boldsymbol{y} \in Y,\ u_y(\boldsymbol{y}+Y) = u_y(\boldsymbol{y})\}$ denotes the function space of periodic functions defined in unit cell Y, $\overline{\chi}$ represents the virtual displacement. Considering the symmetry of the modulus tensor G_{ijkl} and χ_m^{kl}, that is $G_{ijkl} = G_{jikl} = G_{ijlk} = G_{klij}$ and $\chi_m^{kl} = \chi_m^{lk}$, we define $\boldsymbol{G}$ and $\boldsymbol{\chi}$ as the matrix forms of elastic moduli and characteristic displacement expressed in contracted Voigt notation. The components of these matrix are obtained from G_{ijkl} and χ_m^{kl} by following the

replacement of *ij* or *kl*: $11 \to 1$ $22 \to 2$ $33 \to 3$ $23 \to 4$ $13 \to 5$ $12 \to 6$.We seek the solution of the characteristic displacement χ_m^{kl} in the finite dimensional space:

$$\chi_m^{kl}(\boldsymbol{y}) = \sum_i^{Nn} N^i(\boldsymbol{y}) \chi_m^{*i(kl)}, \tag{25}$$

where $N^i(\boldsymbol{y})$ denotes the shape function of node i within the discretization of the characteristic volume; Nn denotes the total number of nodes, and $\chi_m^{*i(kl)}$ is the nodal coefficients. For 2D problems, (*kl*)=(11,22,12); for 3D problems, (*kl*)=(11,22,33,12,13,23). Following the standard Bubnov-Galerkin setting, v_i is defined similarly to equation (25). Substituting the discretization of the influence function and the weight function into the weak form and expressing the terms in matrix–vector form using the Voigt notation yields the following discrete system:

$$\boldsymbol{K}\boldsymbol{\chi}^* = \boldsymbol{f}, \tag{26}$$

where $\boldsymbol{\chi}^*$ is the nodal displacement matrix, $\boldsymbol{K}$ and $\boldsymbol{f}$ are the stiffness matrix and the force matrix, respectively, which are formed by assembling the element matrices:

$$\boldsymbol{K} = \sum_e \int_{Ye} \boldsymbol{B}^T \boldsymbol{G}(\omega, \boldsymbol{y}) \boldsymbol{B} d\boldsymbol{y}, \tag{27}$$

$$\boldsymbol{f} = \sum_e \int_{Ye} \boldsymbol{B}^T \boldsymbol{G}(\omega, \boldsymbol{y}) \boldsymbol{\varepsilon}^0 d\boldsymbol{y}\ , \tag{28}$$

where $\boldsymbol{\varepsilon}^0$ corresponds to the unit strain fields, $\boldsymbol{B}$ is the strain-displacement matrix in element. Take the 2D problem for example:

$$\boldsymbol{B} = \left[\boldsymbol{B}^{[1]} \quad \boldsymbol{B}^{[2]} \quad \dots \quad \boldsymbol{B}^{[Me]}\right],\ \boldsymbol{B}^{[i]} = \begin{bmatrix} N_{,y_1}^{[i]}(\boldsymbol{y}) & 0 & N_{,y_2}^{[i]}(\boldsymbol{y}) \\ 0 & N_{,y_2}^{[i]}(\boldsymbol{y}) & N_{,y_1}^{[i]}(\boldsymbol{y}) \end{bmatrix}^T, \tag{29}$$

in which *T* denotes the matrix transpose, *Me* denotes the total number of nodes in each element. Define $\overline{\boldsymbol{\chi}}^{*(kl)}$ as the *kl*-th column in the matrix $\overline{\boldsymbol{\chi}}^*$ and by rewriting the complex matrix and vectors $\boldsymbol{K}$, $\boldsymbol{\chi}^{*(kl)}$ and $\boldsymbol{f}^{kl}$ in the terms of real and imaginary parts

$$\boldsymbol{K} = \boldsymbol{K}_1 + i\boldsymbol{K}_2, \tag{30}$$

$$\boldsymbol{\chi}^{*(kl)} = \boldsymbol{\chi}_1^{*(kl)} + i\boldsymbol{\chi}_2^{*(kl)}, \tag{31}$$

$$\boldsymbol{f}^{kl} = \boldsymbol{f}_1^{kl} + i\boldsymbol{f}_2^{kl}, \tag{32}$$

the equation (26) can be written as

$$(\boldsymbol{K}_1 + i\boldsymbol{K}_2)\left(\boldsymbol{\chi}_1^{*(kl)} + i\boldsymbol{\chi}_2^{*(kl)}\right) = \boldsymbol{f}_1^{kl} + i\boldsymbol{f}_2^{kl}, \tag{33}$$

where the stiffness matrix and the force vector are written as

$$\boldsymbol{K}_1 = \sum_e \int_{Ye} \boldsymbol{B}^T \boldsymbol{G}'\ (\omega, \boldsymbol{y}) \boldsymbol{B} d\boldsymbol{y}, \quad \boldsymbol{K}_2 = \sum_e \int_{Ye} \boldsymbol{B}^T \boldsymbol{G}''(\omega, \boldsymbol{y}) \boldsymbol{B} d\boldsymbol{y}, \tag{34}$$

$$\boldsymbol{f}_1^{kl} = \sum_e \int_{Ye} \boldsymbol{B}^T \boldsymbol{G}'\ (\omega, \boldsymbol{y}) \boldsymbol{\varepsilon}^{0(kl)} d\boldsymbol{y}, \quad \boldsymbol{f}_2^{kl} = \sum_e \int_{Ye} \boldsymbol{B}^T \boldsymbol{G}''(\omega, \boldsymbol{y}) \boldsymbol{\varepsilon}^{0(kl)} d\boldsymbol{y}, \tag{35}$$

It should be noted that the equation (33) should be solved under the periodic boundary conditions. The effective homogenized viscoelastic complex modulus defined in equation (22) at a

given frequency then can be computed by

$$\boldsymbol{G}^H(\omega) = \frac{1}{|Y|}\int_Y \left(\boldsymbol{G}(\omega, y) - \boldsymbol{G}(\omega, y)\boldsymbol{\varepsilon}_y(\boldsymbol{\chi}^*)\right) \mathrm{dY}. \tag{36}$$

4 New implementation algorithm of the AH of viscoelasticity

In the past section, the finite-element formulation for obtaining the effective complex modulus by the asymptotic homogenization method is derived. Firstly, the characteristic displacement fields $\boldsymbol{\chi}^{*(kl)}$ are obtained by solving equation (33). Subsequently, substituting $\boldsymbol{\chi}^{*(kl)}$ into equation (36) provides the effective complex modulus. But the formulations of the unit cell problems given previously [equations (33)–(36)] remain difficult to solve for the force vector and the stiffness matrix are element type-related. Various element types (e.g. solid, beam, shell, and mixed, must be written for the different microstructures.

This section presents a novel reformulation and numerical algorithm for obtaining the effective complex modulus $\boldsymbol{G}^H(\omega)$ by using the commercial software as a black box. In the new method, an equivalent harmonic analysis is established and a double-layer elements method is proposed to solve the local problem in the homogenization process. The instructions for the process are detailed below.

4.1 Implementation of and formulation of the force vector

In order to achieve the force vector (33) in commercial software, the equation (28) is re-written as

$$\begin{aligned}\boldsymbol{f}_1^{kl} &= \sum_e \int_{Y^e} \boldsymbol{B}^T \mathbf{G}(\omega, \boldsymbol{y})\boldsymbol{\varepsilon}^{0(kl)} d\boldsymbol{y} \\ &= \sum_e \int_{Y^e} \boldsymbol{B}^T \mathbf{G}(\omega, \boldsymbol{y})\left(\boldsymbol{B}\boldsymbol{\chi}_e^{0(kl)}\right) d\boldsymbol{y} \\ &= \sum_e \left(\int_{Y^e} \boldsymbol{B}^T \mathbf{G}(\omega, \boldsymbol{y})\mathbf{B} d\boldsymbol{y}\boldsymbol{\chi}_e^{0(kl)}\right) \\ &= \boldsymbol{K}\boldsymbol{\chi}^{0(kl)},\end{aligned} \tag{37}$$

where $\boldsymbol{\chi}^{0(kl)}$ is the nodal displacement vector corresponding to the unit strain field $\boldsymbol{\varepsilon}^{0(kl)}$, which, for every node, can be written as follows.

$$2D\ problem:\ \ \boldsymbol{\chi}_i^{0(11)} = \begin{Bmatrix} x_i \\ 0 \end{Bmatrix},\ \boldsymbol{\chi}_i^{0(22)} = \begin{Bmatrix} 0 \\ y_i \end{Bmatrix},\ \ \boldsymbol{\chi}_i^{0(12)} = \begin{Bmatrix} 0.5y_i \\ 0.5x_i \end{Bmatrix}, \tag{38}$$

$$3D\ problem:\ \boldsymbol{\chi}_i^{0(11)}=\begin{Bmatrix}x_i\\0\\0\end{Bmatrix},\ \boldsymbol{\chi}_i^{0(22)}=\begin{Bmatrix}0\\y_i\\0\end{Bmatrix},\ \boldsymbol{\chi}_i^{0(33)}=\begin{Bmatrix}0\\0\\z_i\end{Bmatrix},\ \boldsymbol{\chi}_i^{0(12)}=\begin{Bmatrix}0.5y_i\\0.5x_i\\0\end{Bmatrix},\ \boldsymbol{\chi}_i^{0(13)}=\begin{Bmatrix}0.5z_i\\0\\0.5x_i\end{Bmatrix},\ \boldsymbol{\chi}_i^{0(23)}=\begin{Bmatrix}0\\0.5z_i\\0.5y_i\end{Bmatrix}. \tag{39}$$

Here, $\boldsymbol{\chi}_i^{0(kl)}$ is the nodal displacement vector of *i*-th node corresponding to the (*kl*)-th case, and x_i,y_i,z_i are the nodal coordinates of the *i*-th node. Rewriting equation (37) in the terms of the real and imaginary parts, we obtain the following:

$$\boldsymbol{f}_1^{kl}=\boldsymbol{K}_1\boldsymbol{\chi}^{0(kl)};\quad \boldsymbol{f}_2^{kl}=\boldsymbol{K}_2\boldsymbol{\chi}^{0(kl)}. \tag{40}$$

In commercial software, the displacement $\boldsymbol{\chi}^{0(kl)}$ can be applied on the nodes, and the static analysis for the two elastic problems is ran under the prescribed displacement with the material elastic constitute $\boldsymbol{G}'(\omega)$ and $\boldsymbol{G}''(\omega)$, respectively, to achieve the corresponding nodal reaction force $\boldsymbol{f}_1^{kl}$ and $\boldsymbol{f}_2^{kl}$.

4.2 Reformulation and implementation to obtain the characteristic displacement

4.2.1 Equivalent harmonic response analysis model

After calculating the nodal force vector $\boldsymbol{f}^{kl}=\boldsymbol{f}_1^{kl}+i\boldsymbol{f}_2^{kl}$ by equation (40), the finite element equation (33) should be solved to obtain the characteristic displacement fields $\boldsymbol{\chi}^{*(kl)}$. To solve this equation, a harmonic response analyses model is established:

$$(\bar{\boldsymbol{K}}-\bar{\omega}^2\bar{\boldsymbol{M}}+i\bar{\omega}\bar{\boldsymbol{C}})\left(\boldsymbol{u}_1^{kl}+i\boldsymbol{u}_2^{kl}\right)=\boldsymbol{f}_1^{kl}+i\boldsymbol{f}_2^{kl} \tag{41}$$

where $\bar{\boldsymbol{K}}$ represents the structural stiffness matrix; $\bar{\boldsymbol{M}}$ represents the structural mass matrix and $\bar{\boldsymbol{C}}$ represents the structural damping matrix; $\bar{\omega}$ is the circular frequency of the force; and $\boldsymbol{u}_1^{kl}$ and $\boldsymbol{u}_2^{kl}$ are the real displacement vector and the imaginary displacement vector, respectively. By comparing equations (33) and (41), and defining as follows:

$$\bar{\boldsymbol{K}}=\boldsymbol{K}_1;\quad \bar{\boldsymbol{M}}=0;\quad \bar{\boldsymbol{C}}=\frac{\boldsymbol{K}_2}{\bar{\omega}}; \tag{42}$$

the following is obtained:

$$\boldsymbol{\chi}_1^{*(kl)}=\boldsymbol{u}_1^{kl};\quad \boldsymbol{\chi}_2^{*(kl)}=\boldsymbol{u}_2^{kl}. \tag{43}$$

In this way, the problem of solving the complex linear equation (33) is transformed into solving a harmonic response analysis (41). Next, the discussion focuses on establishing the formulations (42) through the use of commercial software. By setting the elastic material properties as $\mathbf{G}'(\omega)$, the material density as 0, then the structural stiffness matrix $\bar{\boldsymbol{K}}$ equals $\widetilde{\boldsymbol{K}}_1$, and the structural mass

matrix $\bar{\mathbf{M}}$ equals to the zero matrix. However, the ability to define $\mathbf{C} = \widetilde{\boldsymbol{K}}_2/\omega$ though the use of commercial software remains difficult because of the lack of damping models. To solve this challenge, equation (33) is modified to the form:

$$\left((\boldsymbol{K}_1 + \varsigma\boldsymbol{K}_2) + i\left(0 \times \boldsymbol{K}_1 + \varsigma \times \frac{1}{\varsigma}\boldsymbol{K}_2\right)\right)\left(\boldsymbol{\chi}_1^{*(kl)} + i\boldsymbol{\chi}_2^{*(kl)}\right) = \boldsymbol{f}_1^{kl} + i\boldsymbol{f}_2^{kl}, \tag{44}$$

where ς is a small positive number $(0 < \varsigma \leq 1)$ to ensure that $(\boldsymbol{K}_1 + \varsigma\boldsymbol{K}_2) \approx \boldsymbol{K}_1$ and $0 \times \boldsymbol{K}_1 + \varsigma \times \frac{1}{\varsigma}\boldsymbol{K}_2 \equiv \boldsymbol{K}_2$, hence this equation shares the same solution of equation (33). The reason for constructing this approximate formulation is mainly to establish a *weak* linear relationship between the real part and the imaginary part. "*Weak*" here means that each terms in the two parts have a linear relationship, such as the first term in the real part $\boldsymbol{K}_1$ and second first term $0 \times \boldsymbol{K}_1$ in the real part is linear with the coefficient 0, similarly, the second term in the real part $\varsigma \times \frac{1}{\varsigma}\boldsymbol{K}_2$ and second first term $\varsigma \times \frac{1}{\varsigma}\boldsymbol{K}_2$ in the real part is linear with the coefficient ς. In this way, the proportional damping model which is widely applied in commercial software can be used. By comparing equations (44) and the harmonic response model (41), the following is defined

$$\bar{\boldsymbol{K}} = \boldsymbol{K}_1 + \varsigma\boldsymbol{K}_2\,; \quad \bar{\boldsymbol{M}} = 0 \times \boldsymbol{M}_1 + 0 \times \boldsymbol{M}_2\,; \quad \bar{\boldsymbol{C}} = \frac{1}{\bar{\omega}}\left(0 \times \boldsymbol{K}_1 + \frac{1}{\varsigma} \times \varsigma\boldsymbol{K}_2\right). \tag{45}$$

It should be noted that the methodology holds for any $\bar{\omega}$ and for simplicity, we take $\bar{\omega} = 1$ is used in this paper; hence formulae (45) can be rewritten as

$$\bar{\boldsymbol{K}} = \boldsymbol{K}_1 + \varsigma\boldsymbol{K}_2\,; \quad \bar{\boldsymbol{M}} = 0 \times \boldsymbol{M}_1 + 0 \times \boldsymbol{M}_2\,; \quad \bar{\boldsymbol{C}} = 0 \times \boldsymbol{K}_1 + \frac{1}{\varsigma} \times \varsigma\boldsymbol{K}_2. \tag{46}$$

In this way, the local problem (33) is transformed to an equivalent harmonic response equation (41) with the stiffness, mass and damping matrices defined by equation (46). In next section, a double-layer elements method is proposed for establishing the model defined in formulation (46) and then the harmonic response problem can be solved easily by the readily available subroutine in commercial software.

4.2.2 Double-layer elements method

Rewrite equation (46) at an element-level:

$$\bar{\boldsymbol{K}}^e = \boldsymbol{K}_1^e + \varsigma\boldsymbol{K}_2^e\,; \quad \bar{\boldsymbol{M}}^e = 0 \times \boldsymbol{M}_1^e + 0 \times \boldsymbol{M}_2^e\,; \quad \bar{\boldsymbol{C}}^e = 0 \times \boldsymbol{K}_1^e + \frac{1}{\varsigma} \times \varsigma\boldsymbol{K}_2^e, \tag{47}$$

where the superscript *e* denotes the element matrix. By observing this formulation, it is apparent that all the matrices are sums of two parts. Here, a double-layer elements method is proposed for modeling the summation of the element stiffness, damping and mass matrices. The basic idea is that, for each mesh, there are two elements on two layers, which share the common nodes but have

different material properties. As shown in Fig. 2, Element 1 (first-layer element) and Element 2 (second-layer element) share the common Mesh 1 with Nodes 2, 5, 4 and 1. Therefore, for each mesh, the stiffness (damping or mass) matrix of the mesh will be summed by two element-stiffness (damping or mass) matrices:

$$\boldsymbol{k}_m = \boldsymbol{k}_{1e} + \boldsymbol{k}_{2e}. \tag{48}$$

This method can be realized through most commercial software, *e.g.*, *ANSYS*. One efficient way is to discrete the *CAD* model, copy all the elements, and then merge the nodes that share the same locations.

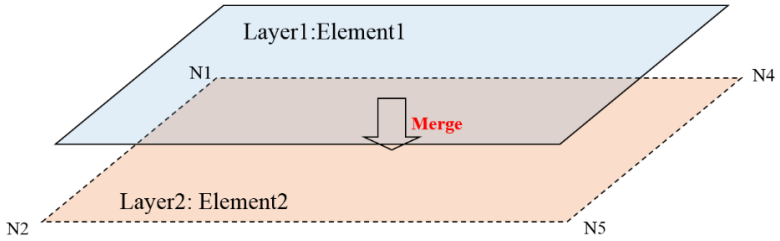

(a) A mesh with two elements which shares the same nodes

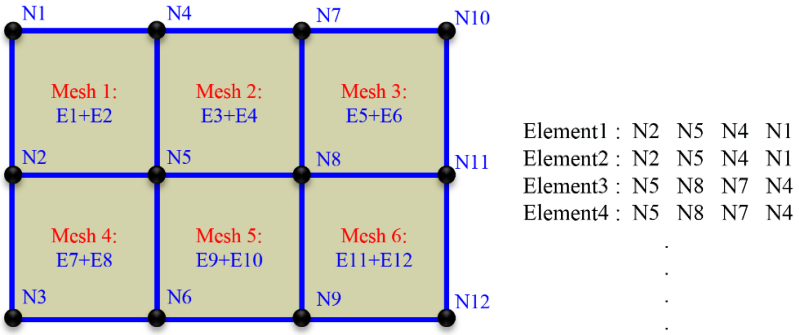

(b) Illustration of the final finite element model

Fig. 2 Illustration of the double-layer elements method.

The properties of the material assigned to the first-layer elements are $\boldsymbol{G}'(\omega)$ (the storage modulus) as the elastic modulus, the density at zero, and the damping ratio. The ones assigned to the second-layer elements are $\varsigma\boldsymbol{G}''(\omega)$ (ς times the loss modulus) as the elastic modulus, the density at zero, and the damping ratio $1/\varsigma$. It should be noted that, in practice, both of the material densities of the two elements equal ρ_ε ($\rho_\varepsilon \ll 1$), a small positive number, prevents singularity. The material properties for the elements on these two layers are defined and given in Table 1.

Table 1 Material properties of the two layers

Layer	Material elastic matrix	Material density	Material damping ratio
Layer 1	$\boldsymbol{G}'(\omega)$	ρ_ε	0
Layer 2	$\varsigma\boldsymbol{G}''(\omega)$	ρ_ε	$1/\varsigma$

By following the setting of the material properties in the commercial software, the nodal force vector $\boldsymbol{f}^{kl} = \boldsymbol{f}_1^{kl} + i\boldsymbol{f}_2^{kl}$ is computed by equation (40) for all the nodes, and the finite-element model [equation (44)] under periodic boundary conditions can be solved by the harmonic response analyses. The characteristic displacement field $\boldsymbol{\chi}^{*(kl)} = \boldsymbol{\chi}_1^{*(kl)} + i\boldsymbol{\chi}_2^{*(kl)}$ can be obtained directly from the outputs provided by the software.

4.3 Implementation of obtaining effective complex moduli

The effective viscoelastic complex modulus formulated by equation (36) can also be expressed in the form of strain energy (56, 57):

$$\boldsymbol{G}^H = \frac{1}{|Y|}\int_Y (\boldsymbol{\varepsilon}^0 - \boldsymbol{\varepsilon}_y(\boldsymbol{\chi}^*))^T \boldsymbol{G}(\boldsymbol{\varepsilon}^0 - \boldsymbol{\varepsilon}_y(\boldsymbol{\chi}^*))\, dY. \tag{49}$$

The physical meaning of this formulation is the strain energy of unit cell; in which the corresponding strain equals the difference between the unit strain and the characteristic strain. Thus, Eq. (49) can be rewritten in the matrix form as

$$\boldsymbol{G}^H = \frac{1}{|Y|}(\boldsymbol{\chi}^0 - \boldsymbol{\chi}^*)^T \boldsymbol{K}(\boldsymbol{\chi}^0 - \boldsymbol{\chi}^*) = \frac{1}{|Y|}(\boldsymbol{\chi}^0 - \boldsymbol{\chi}^*)^T(\boldsymbol{f} - \boldsymbol{f}^*), \tag{50}$$

where $\boldsymbol{\chi}^0, \boldsymbol{\chi}^*$, $\boldsymbol{f}$ and $\boldsymbol{f}^*$ are complex matrices, which are assembled by $\boldsymbol{\chi}^{0(kl)}, \boldsymbol{\chi}^{*(kl)}$, $\boldsymbol{f}^{(kl)}$ and $\boldsymbol{f}^{*(kl)}$, respectively. Of which $\boldsymbol{\chi}^{0(kl)}, \boldsymbol{\chi}^{*(kl)}$, and $\boldsymbol{f}^{(kl)}$ have been obtained by equations (38) or (39), equation (44) and equation (24), respectively, and $\boldsymbol{f}^{*(kl)}$ is defined as

$$\boldsymbol{f}^{*(kl)} = \boldsymbol{f}_1^{*(kl)} + i\boldsymbol{f}_2^{*(kl)}.$$

$$\boldsymbol{f}_1^{*(kl)} = \boldsymbol{K}_1\boldsymbol{\chi}_1^{*(kl)} - \boldsymbol{K}_2\boldsymbol{\chi}_2^{*(kl)}; \quad \boldsymbol{f}_2^{*(kl)} = \boldsymbol{K}_1\boldsymbol{\chi}_2^{*(kl)} + \boldsymbol{K}_2\boldsymbol{\chi}_1^{*(kl)}. \tag{51}$$

All the quantities in these equations are either given or are outputs direct from the commercial software and are prepared for calculating the effective stiffness coefficients of the structure in the commercial software.

5 Flow chart

To better illustrate our method, Fig. 3 provides a flowchart:

Step 1. Establish the finite-element model of the unit cell by using commercial software.

Step 2. Apply nodal displacement fields $\boldsymbol{\chi}^{0(kl)}$ given in equation (38) or (39) on each node.

Set the material elastic property as storage modulus $\boldsymbol{G'}$; run one static analysis for each condition (solve the equation (40)); and get the corresponding nodal reaction force $\boldsymbol{f}_1^{kl}$. Then, modify the material elastic property to loss modulus $\boldsymbol{G''}$ and perform the same computation to obtain the nodal reaction force $\boldsymbol{f}_2^{kl}$. Thus, the nodal force vector $\boldsymbol{f}^{kl} = \boldsymbol{f}_1^{kl} + i\boldsymbol{f}_2^{kl}$ is obtained.

Step 3. Establish a new finite-element model by executing the double-layer elements method described in Section 3.2. Then apply nodal reaction force $\boldsymbol{f}^{kl}$ on each node, run a harmonic response analysis with periodic boundary conditions (solve the equation (44)), and obtain the characteristic displacement field $\boldsymbol{\chi}^{*(kl)}(= \boldsymbol{\chi}_1^{*(kl)} + i\boldsymbol{\chi}_2^{*(kl)})$. After which, $\boldsymbol{\chi}_1^{*(kl)}$ and $\boldsymbol{\chi}_2^{*(kl)}$ are obtained. Merge all elements, which share the same mesh.

Step 4. Apply the characteristic displacement field $\boldsymbol{\chi}^{*(kl)}$ on each node. Set the material elastic property of the element as storage modulus $\boldsymbol{G'}$; run the static analysis again; and obtain the nodal reaction force $\boldsymbol{K}_1\boldsymbol{\chi}_1^{*(kl)}$. Similarly, $\boldsymbol{K}_1\boldsymbol{\chi}_2^{*(kl)}$,$\boldsymbol{K}_2\boldsymbol{\chi}_2^{*(kl)}$and $\boldsymbol{K}_2\boldsymbol{\chi}_1^{*(kl)}$can also be obtained. According to equation (51), obtain the force vector $\boldsymbol{f}^{*(kl)} = \boldsymbol{f}_1^{*(kl)} + i\boldsymbol{f}_2^{*(kl)}$.

Step 5. Calculate the effective complex modulus matrix by $\boldsymbol{G}^H = \frac{1}{|Y|}(\boldsymbol{\chi}^0 - \boldsymbol{\chi}^*)^T(\boldsymbol{f} - \boldsymbol{f}^*)$ [equation (50)].

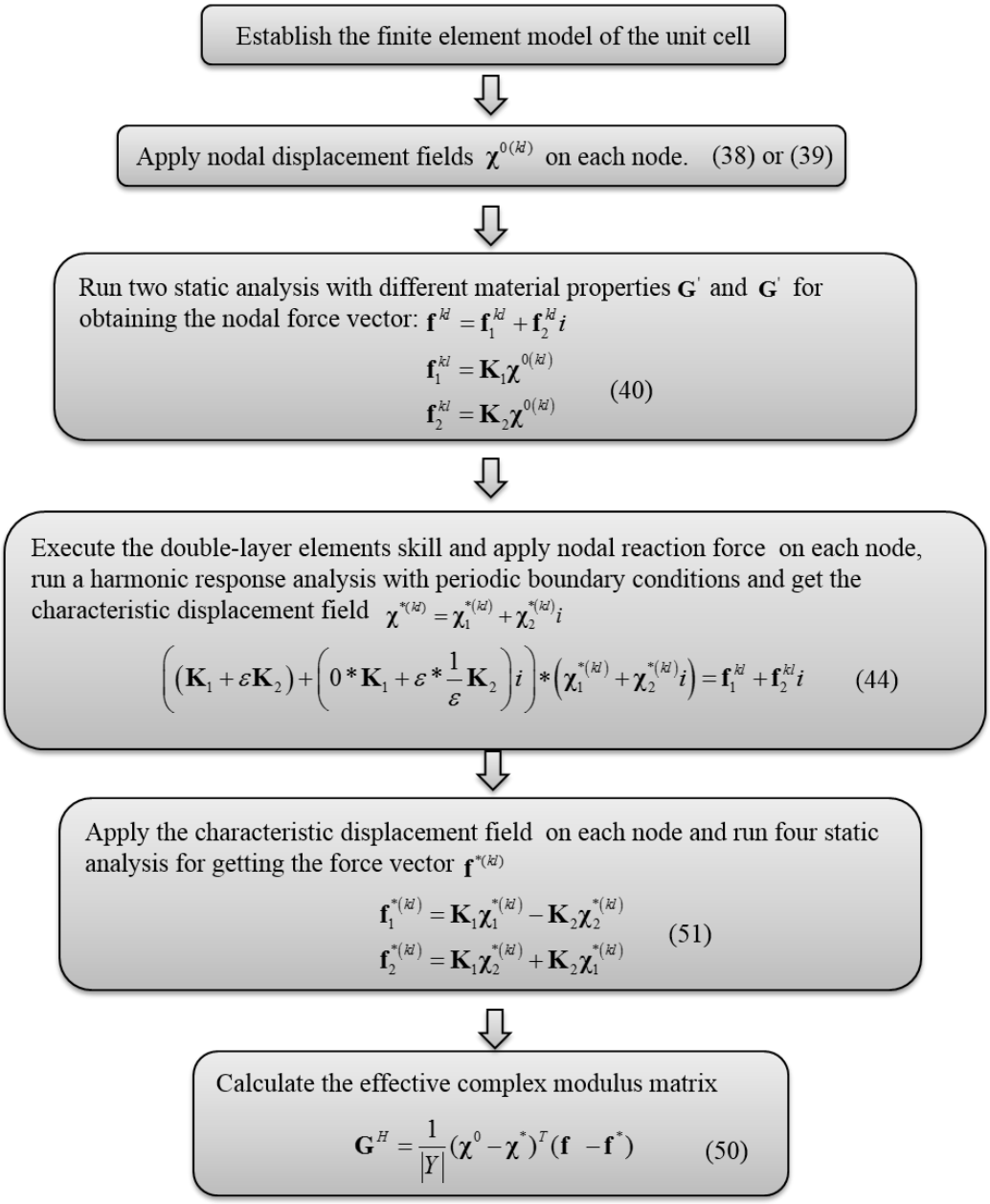

Fig. 3 Flowchart of the new implementation of asymptotic homogenization

6 Numerical examples

In this section, to demonstrate the effectiveness of the new implementation of the AH method in predicting the viscoelastic modulus of periodic composite materials, three examples are examined by using the commercial software *ANSYS*.

6.1 Particle-reinforced composite

As the first example, the effective viscoelastic responses of particle-reinforced composite with circular inclusions in a square matrix are computed by using the novel implementation method

outlined previously. Assume the constituent materials are assumed isotropic and the volume fraction of the inclusion is 50%. The finite element mesh for the microstructure is shown in Fig. 4. This model has been solved by traditional implementation in (32). To validate our proposed method, we use two different material properties of matrix and inclusion, and the results obtained by the new implementation are compared to the results given by Yi *et al.*

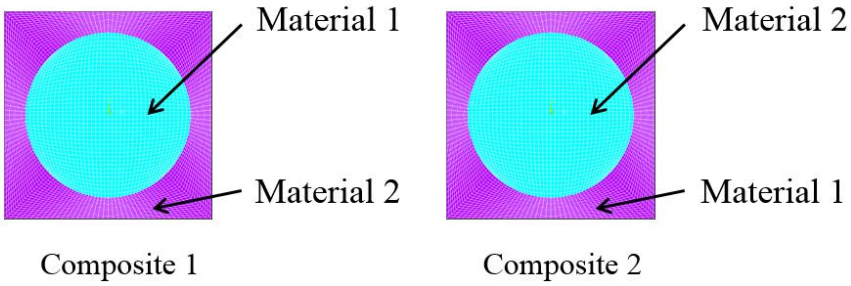

Fig. 4 Illustration of the finite element mesh of the microstructures

First, a viscoelastic composite with elastic circular inclusion in the viscoelastic matrix (Composite 1) and a viscoelastic composite with a viscoelastic circular inclusion in the elastic matrix (Composite 2) are considered, respectively. The material properties of the elastic inclusions (Material 1) are

$$E = 70GPa,\ v = 0.22. \tag{52}$$

The material properties of the viscoelastic matrix (Material 2) are given as

$$E(t) = 1 + 2.5e^{-t}GPa,\ v = 0.35. \tag{53}$$

Table 2 gives a comparison of the results computed by the new implementation of asymptotic homogenization (NIAH) and the results by Yi et al (Ref) (32) for frequency equals to 0.5. It is apparent that the results of new implementation coincide very well with the traditional implementation with the minor errors for different finite-element mesh.

Table 2 Comparison of the results of new implementation and traditional implementation

Microstructure	Frequency (ω)	$G_{11}^{H\prime}$		$G_{11}^{H\prime}$		$tan(\delta)$	
		NIAH	Ref	NIAH	Ref	NIAH	Ref
Material 1	0.5	73.56	73.56	0.00	0.00	0.000	0.000
Material 2	0.5	1.71	1.71	1.14	1.14	0.667	0.667
Composite 1	0.5	4.58	4.64	2.83	2.86	0.618	0.618
Composite 2	0.5	24.84	23.28	1.10	1.14	0.044	0.049

Next, composites with the microstructures composed of two isotropic viscoelastic materials

with different relaxation times are considered. The relaxation moduli are given as follows:

$$E(t) = 0.5 + 3e^{-t/10} GPa,\ v = 0.35\ \ for\ material\ 1. \tag{54}$$

$$E(t) = 0.5 + 3e^{-t} GPa,\ v = 0.35\ \ for\ material\ 2. \tag{55}$$

A similar comparison of the results is given in Table 3. It is apparent again that the results of new implementation coincide very well with the traditional implementation. Fig. 5 shows the loss tangents of the two given constituent materials and the two conventional composites as a function of frequency. The results show that by designing the topology of the microstructure, the preferred damping characteristics of the composite can be obtained within an interesting range of frequency. This can help obtain the maximum damping ratio at fixed frequency.

Table 3 Comparison of results of new implementation and traditional implementation

Microstructure	Frequency (ω)	$G_{11}^{H\prime}$		$G_{11}^{H\prime}$		$tan(\delta)$	
		NIAH	Ref	NIAH	Ref	NIAH	Ref
Material 1	0.04	1.04	1.04	1.18	1.18	1.132	1.132
	0.4	3.79	3.79	0.80	0.80	0.212	0.212
Material 2	0.04	0.58	0.58	0.14	0.14	0.237	0.237
	0.4	1.04	1.04	1.18	1.18	1.132	1.132
Microstructure 1	0.04	0.84	0.84	0.43	0.43	0.510	0.510
	0.4	2.04	2.04	1.36	1.36	0.672	0.670
Microstructure 2	0.04	0.81	0.80	0.52	0.50	0.637	0.625
	0.4	2.14	2.10	1.19	1.20	0.555	0.571

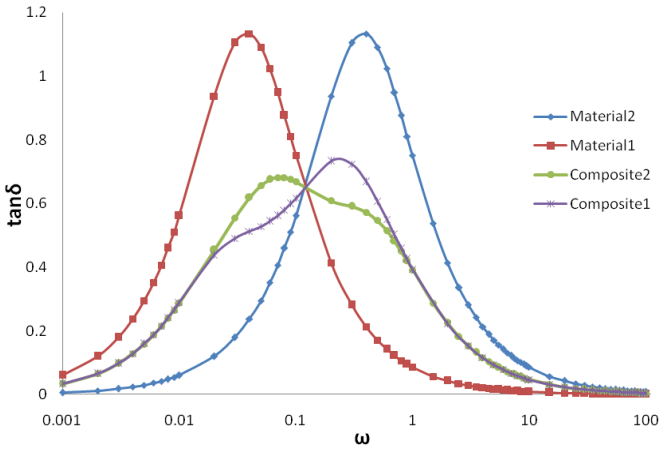

Fig. 5 Variations of loss tangents against frequency ω.

6.2 Fiber reinforced composite

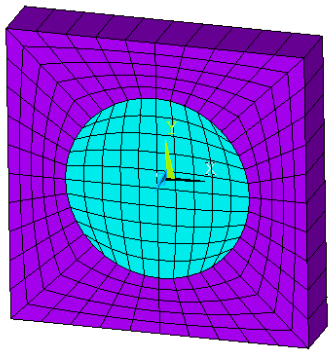

Fig. 6 Unit cell and finite element mesh of fiber reinforced composite.

In this example, a fiber-reinforced composite, whose unit cell is shown in Fig. 6 is considered, and a complete process using the new method to obtain the viscoelastic modulus in the frequency and time domain is presented. The fiber is a transversely isotropic elastic material, whereas, the resin matrix is a viscoelastic material with the constitutive equation:

$$\{S(t)\} = \int_0^t Y(t-\tau)\frac{\partial\{e(\tau)\}}{\partial\tau}d\tau\,,\sigma = 3Ke, \tag{56}$$

where $\{S(t)\}$ is the deviatoric stress tensor; σ is the spherical stress tensor; $e(\tau)$ is the deviatoric strain tensor; and e is the spherical strain tensor. K is the bulk modulus, and its bulk deformation satisfies the elastic behavior. $Y(t)$ is the shear modulus, and its shear deformation satisfies the three-parameter solid model:

$$Y(t) = 2G_1\left[1-\frac{G_1}{G_1+G_2}\left(1-e^{-t\frac{G_2+G_1}{\eta_2}}\right)\right], \tag{57}$$

where G_1,G_2 are the elastic modulus of the viscoelastic material and η_2 is the viscosity coefficient. Fig. 7 illustrates a three-parameter solid model. The shear moduli are written within the time domain, and the complex modulus can be obtained by Fourier transform:

$$Y(\omega) = p + \frac{\omega^2 q}{\alpha^2+\omega^2} + i\left(\frac{\omega q\alpha}{\alpha^2+\omega^2}\right), \tag{58}$$

where $p = G_1\left(1-\frac{G_1}{G_1+G_2}\right)$, $q = \frac{2G_1^2}{G_1+G_2}$ and $\alpha = \frac{G_2+G_1}{\eta_2}$.

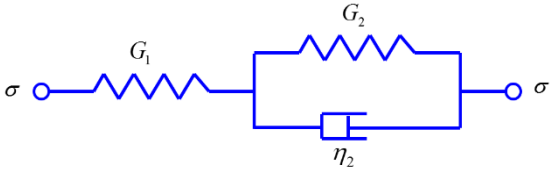

Fig. 7 Illustration of the three-parameter solid model.

The constitutive equation (56) also can be written as:

$$\{\sigma\} = \int_0^t G(t-\tau)\frac{\partial\{\varepsilon(\tau)\}}{\partial\tau}d\tau, \tag{59}$$

where $G(t)$ is the relaxation modulus and can be written in the matrix form:

$$G = \begin{bmatrix} K+\frac{4}{3}Y & K-\frac{2}{3}Y & K-\frac{2}{3}Y & 0 & 0 & 0 \\ K-\frac{2}{3}Y & K+\frac{4}{3}Y & K-\frac{2}{3}Y & 0 & 0 & 0 \\ K-\frac{2}{3}Y & K-\frac{2}{3}Y & K+\frac{4}{3}Y & 0 & 0 & 0 \\ 0 & 0 & 0 & Y & 0 & 0 \\ 0 & 0 & 0 & 0 & Y & 0 \\ 0 & 0 & 0 & 0 & 0 & Y \end{bmatrix}. \tag{60}$$

In this paper, the resin matrix material is ED-6, and the fiber material is graphite fiber T300, whose material constants are presented in Table 4 and Table 5, respectively.

Table 4 Viscoelastic material constants of ED-6 in room temperature

	$G_1(GPa)$	$G_2(GPa)$	$\eta_2(GPa)$	$K(GPa)$
ED-6	3.2	1.8	300	4.44

Table 5 Elastic material constants of T300

	$E_1(GPa)$	$E_2(GPa)$	$G_{12}(GPa)$	$G_{31}(GPa)$	ν_{12}	ν_{13}
T300	13.8	22.1	5.52	9.0	0.25	0.2

Through the new implementation of asymptotic homogenization, the effective moduli of the viscoelastic composite can be computed. Fig. 9 shows the effective modulus G_{11}^H, and damping ratio δ_{11} for fiber volumes fraction equals 0.3. The subscript 'ij' is used to denote the value in the i-th row, j-th column in the matrix (60). From Fig. 9 it is possible to find that the maximum damping ratio occurs at $\omega = 0.12$ and that the damping ratio decreases with the increase of frequency, whereas the storage modules increase for supplying a stiffness.

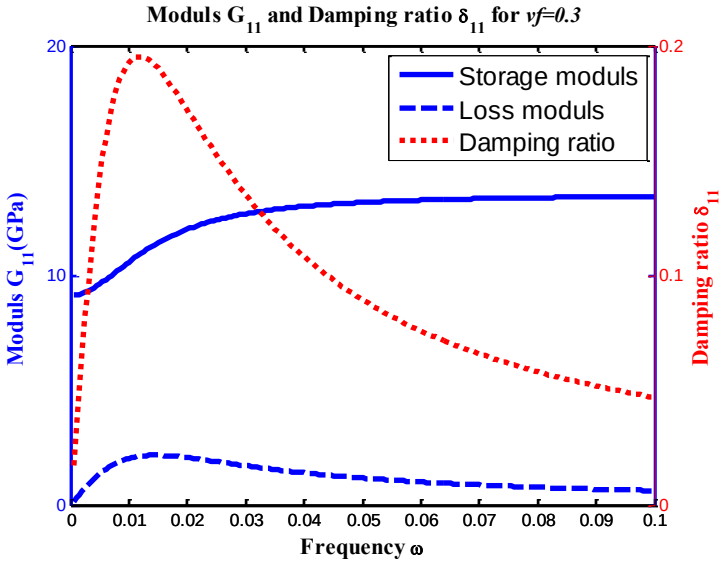

Fig. 8 . Variations of the effective modulus G_{11} and the damping ratio δ_{11} for fiber volume fractions equals 0.3 against frequency ω.

In particular, it can be demonstrated that, by adjusting the volume fraction of the fiber in a matrix, it is possible, in principle, to modify its damping response in the frequency domain. As shown in Fig. 9, the damping ratio decreases while adding the fiber volume fraction. It should be noted that the frequency at which the maximum damping ratio occurs also slightly decreases with the increase in fiber volume fractions.

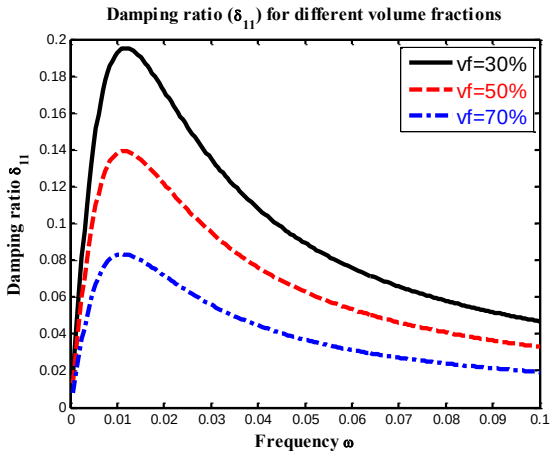

(a)

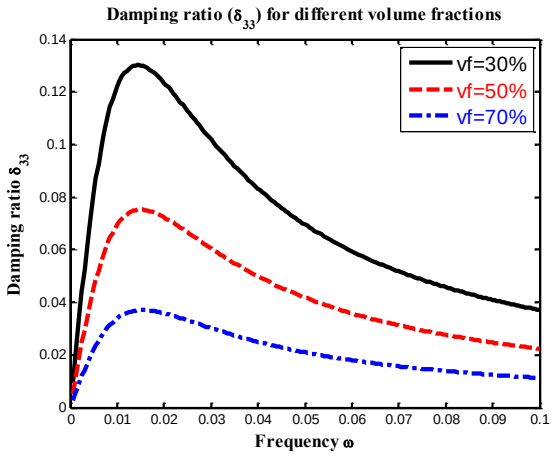

(b)

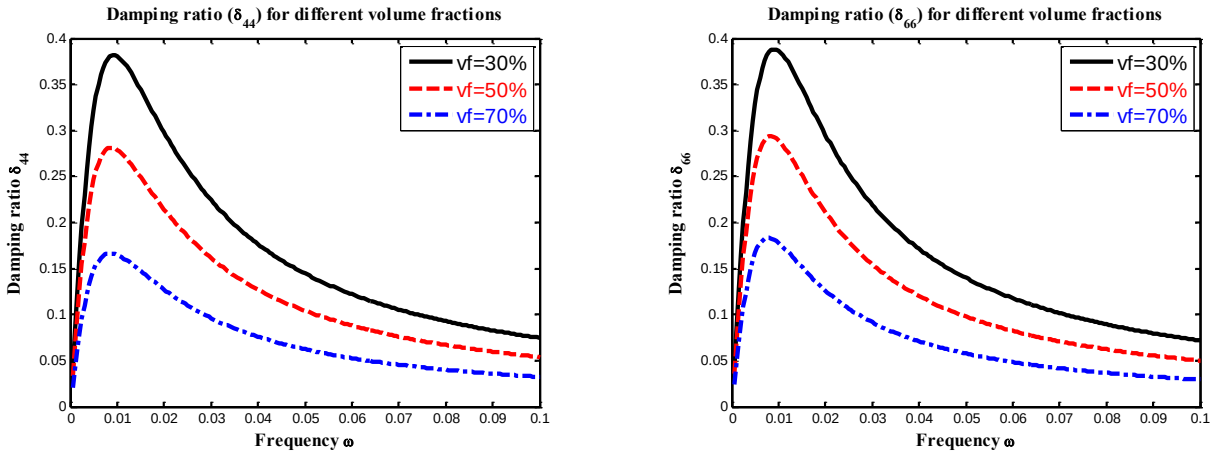

(d) (e)

Fig. 9 Composite of the damping ratios for the different fiber volume fractions: (a) δ_{11}; (b) δ_{33}; (c) δ_{44}; (d) δ_{66}.

Assuming the effective viscoelastic modulus of the composite also satisfies the three-parameter solid model, it follows that

$$G_{ij}^{H}(\omega) = p^{H} + \frac{\omega^2 q^{H}}{\alpha^{H^2}+\omega^2} + i\left(\frac{\omega q^{H}\alpha^{H}}{\alpha^{H^2}+\omega^2}\right). \tag{61}$$

Consequently, the analytical functions of the effective viscoelastic modulus of the composite can be obtained by using a linear least-squares fit to obtain the values of parameters p^H, q^H and α^H. Furthermore, the inverse Fourier transformation is used to obtain the effective viscoelastic modulus in the time domain (as shown in Fig. 10).

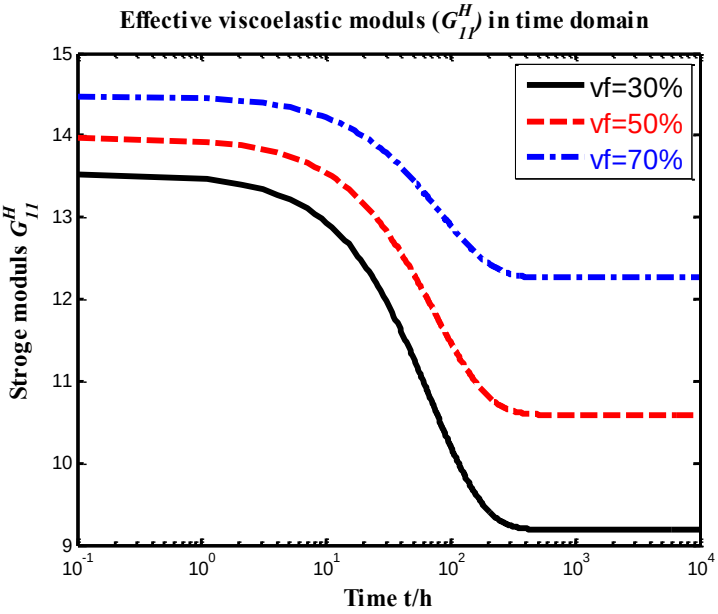

Fig. 10 Effective viscoelastic modulus for different volumes of fiber in the time domain.

6.3 Octet-truss lattice material

In this example, an octet-truss lattice material with the unit cell shown in Fig. 11 is considered. The unit cell consists of an internal octahedral cell (dark color) and eight outer tetrahedral cells (light color), whose effective elastic properties have been investigated through analytical and FE calculations by Deshpande et al (58) and Cheng et al (44). In this paper, the effective viscoelastic moduli are computed for this unit cell, in which all the rods have lengths of 1.0mm, and the cross sections have diameters of 0.1mm.

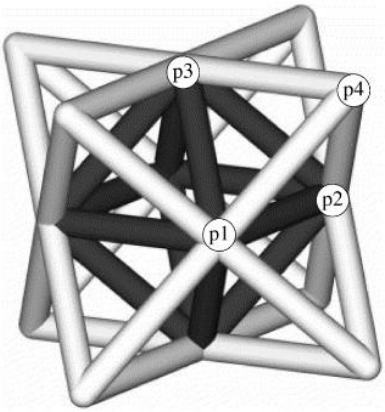

Fig. 11 Unit cell of the octet-truss lattice material consisting of one internal octahedral cell and eight outer tetrahedral cells.

Two types of elements, the tetrahedral solid element and the beam element, are used to establish the finite element models (Fig. 12) of the unit cell. For the finite element discretized by the solid elements, 49,784 elements and 169,048 elements are used for the two different mesh sizes. Whereas, for the finite element discretized by the beam elements, only 360 elements are used. Assume the unit cell is a homogeneous isotropic viscoelastic material with Young's modulus $E = (1.5 + i * 1)GPa$ and Poisson's ratio $v = 0.35$. The effective complex moduli of the octet–truss lattice material can be computed for these three finite-element models; the results are presented in Table 6. It is apparent that the results obtained by the beam element model are close to those of the solid-element models. However, the solid-element models used a large number of tetrahedral elements to achieve sufficient accuracy, and the beam-element model used only a few beam elements. Finer mesh in the unit cell results in a convergence with the result from the beam-element model; however, the computing time for the solid-element models is much longer.

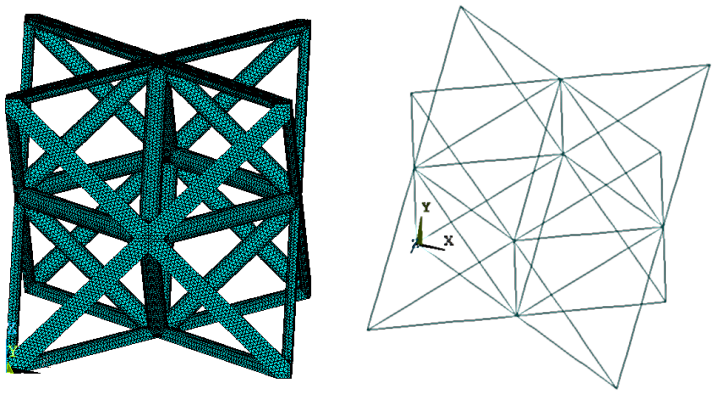

(a) (b)

Fig. 12 Finite element of the unit cell. (a) solid element; (b) beam element.

Table 6 Effective complex moduli of octet-truss lattice material for the three finite element models

Mesh	Element Number	$G_{11}^{H\prime}$	$G_{11}^{H\prime\prime}$	$tan(\delta_{11})$	$G_{44}^{H\prime}$	$G_{44}^{H\prime\prime}$	$tan(\delta_{44})$
Beams	360	1.68e-2	1.12e-2	0.666	8.39e-2	5.59e-2	0.666
Tetrahedral	49784	1.92e-2	1.28e-2	0.666	9.02e-2	6.01e-2	0.666
	169048	1.88e-2	1.25e-2	0.666	8.86e-2	5.91e-2	0.666

Next, by assuming that the unit cell is heterogenetic, the internal octahedral cell consists of an isotropic elastic material with the properties $E^i = 70GPa$, $v^i = 0.22$, whereas, the eight outer tetrahedral cells consists of viscoelastic material with the properties $E^o = 1 + 2.5e^{-t}GPa$, $v^o = 0.35$. The beam-element model is used to compute the effective complex modulus for simplicity and efficiency. Fig. 13 shows the variations of effective modulus G_{11} and the damping ratio δ_{11} with ω for the octet-truss material. Because the loss modulus is much lower than that of the storage modulus of the composite, the variation tendency of the damping ratio against the frequency is similar to that of the loss modulus.

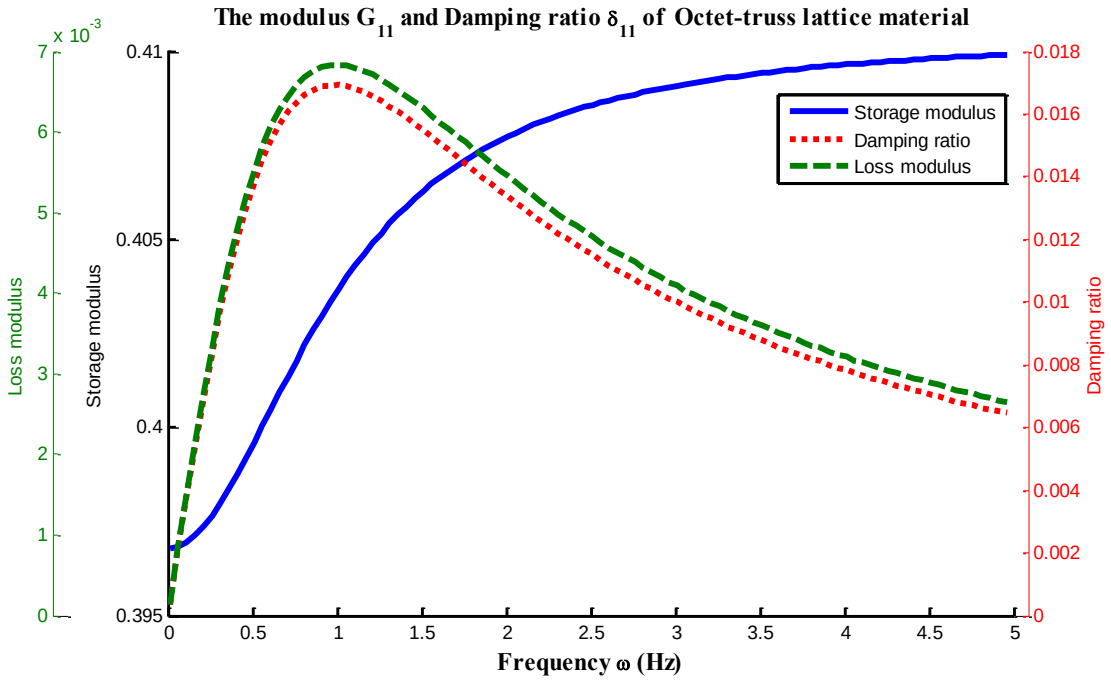

Fig. 13 Variation of the effective modulus G_{11} and the damping ratio δ_{11} with ω for octet-truss material.

7 Conclusions

In this paper, a novel numerical implementation algorithm of the asymptotic homogenization theory for predicting the effective complex moduli of a composite in the frequency domain is proposed. To solve the local problem in the homogenization process, an equivalent harmonic analysis is performed, and a double-layer elements method is proposed. Through this algorithm, the viscoelastic response of the composites in the frequency domain can be obtained easily by using commercial software in a black-box role. In this way, the powerful modeling and analytical abilities of the commercial software are utilized for computing complicated unit cells. The viscoelastic properties of the particle-reinforced composites, the fiber-reinforced composites, and the octet-truss lattice materials are computed with this method to illustrate the effectiveness and simplicity of this new implementation.

Acknowledgements

The authors gratefully acknowledge the financial support to this work by the National Natural Science Foundation of China (Grant Nos. 11332004 and 11172052), the National Basic Research Program of China (Grant No. 2011CB610304), the 111 Project (B14013), the Fundamental Research Funds for the Central Universities of China (DUT15ZD101) and the Fundamental Research Funds of Shandong University.

References

1. Jang JL, Tarng YS. A study of the active vibration control of a cutting tool. Journal of Materials Processing Technology. 1999;95(1–3):78-82.

2. Taniwangsa W, Kelly JM, editors. Experimental testing of a semi-active control scheme for vibration suppression1997.

3. Raja S, Rohwer K, Rose M. Piezothermoelastic modeling and active vibration control of laminated composite beams. Journal of intelligent material systems and structures. 1999;10(11):890-9.

4. Rao MD. Recent applications of viscoelastic damping for noise control in automobiles and commercial airplanes. Journal of Sound and Vibration. 2003;262(3):457-74.

5. Lakes R. High damping composite materials: effect of structural hierarchy. Journal of composite materials. 2002;36(3):287-97.

6. Chen W, Liu S. Microstructural topology optimization of viscoelastic materials for maximum modal loss factor of macrostructures. Structural and Multidisciplinary Optimization. 2015:1-14.

7. Du J, Yang R. Vibro-acoustic design of plate using bi-material microstructural topology optimization. Journal of Mechanical Science and Technology. 2015;29(4):1413-9.

8. Patel RK, Bhattacharya B, Basu S. A finite element based investigation on obtaining high material damping over a large frequency range in viscoelastic composites. Journal of Sound and Vibration. 2007;303(3–5):753-66.

9. Dong L, Lakes R. Advanced damper with high stiffness and high hysteresis damping based on negative structural stiffness. International Journal of Solids and Structures. 2013;50(14–15):2416-23.

10. Wang Y, Lakes R. Extreme stiffness systems due to negative stiffness elements. American Journal of Physics. 2004;72(1):40-50.

11. Aboudi J. Mechanics of composite materials-A unified micromechanical approach. NASA STI/Recon Technical Report A. 1991;93.

12. Nemat-Nasser S, Hori M. Micromechanics: overall properties of heterogeneous materials: Elsevier; 2013.

13. Kanaun S, Levin V. Self-Consistent Methods for Composites: Vol. 1: Static Problems: Springer Science & Business Media; 2007.

14. Huang Y, Hu K, Wei X, Chandra A. A generalized self-consistent mechanics method for composite materials with multiphase inclusions. Journal of the Mechanics and Physics of Solids. 1994;42(3):491-504.

15. Benveniste Y. A new approach to the application of Mori-Tanaka's theory in composite materials. Mechanics of materials. 1987;6(2):147-57.

16. Sun CT, Vaidya RS. Prediction of composite properties from a representative volume element. Composites Science and Technology. 1996;56(2):171-9.

17. Bensoussan A, Lions J-L, Papanicolaou G. Asymptotic analysis for periodic structures: American Mathematical Soc.; 2011.

18. Hori M, Nemat-Nasser S. On two micromechanics theories for determining micro–macro relations in heterogeneous solids. Mechanics of Materials. 1999;31(10):667-82.

19. Lakes RS. Viscoelastic materials: Cambridge University Press; 2009.

20. Hashin Z. Viscoelastic Behavior of Heterogeneous Media. Journal of Applied Mechanics. 1965;32(3).

21. Christensen R. Viscoelastic properties of heterogeneous media. Journal of the Mechanics and Physics of Solids. 1969;17(1):23-41.

22. Wang YM, Weng GJ. The Influence of Inclusion Shape on the Overall Viscoelastic Behavior of Composites. Journal of Applied Mechanics. 1992;59(3):510-8.

23. Luciano R, Barbero EJ. Analytical Expressions for the Relaxation Moduli of Linear Viscoelastic Composites With Periodic Microstructure. Journal of Applied Mechanics. 1995;62(3):786-93.

24. Tran AB, Yvonnet J, He QC, Toulemonde C, Sanahuja J. A simple computational homogenization method for structures made of linear heterogeneous viscoelastic materials. Computer Methods in Applied Mechanics and Engineering. 2011;200(45–46):2956-70.

25. Yi YM, Park SH, Youn SK. Asymptotic homogenization of viscoelastic composites with periodic microstructures. International Journal of Solids & Structures. 1998;35(17):2039–55.

26. Liu S, Chen K-Z, Feng X-A. Prediction of viscoelastic property of layered materials. International Journal of Solids and Structures. 2004;41(13):3675-88.

27. Liu X, Tang T, Yu W, Pipes RB. Multiscale modeling of viscoelastic behaviors of textile composites. International Journal of Engineering Science. 2018;130:175-86.

28. Andreassen E, Jensen JS. Topology optimization of periodic microstructures for enhanced dynamic properties of viscoelastic composite materials. Structural and Multidisciplinary Optimization. 2014;49(5):695-705.

29. Chen W, Liu S. Topology optimization of microstructures of viscoelastic damping materials for a prescribed shear modulus. Structural and Multidisciplinary Optimization. 2014;50(2):287-96.

30. Huang X, Zhou S, Sun G, Li G, Xie YM. Topology optimization for microstructures of viscoelastic composite materials. Computer Methods in Applied Mechanics and Engineering. 2015;283:503-16.

31. Andreasen CS, Andreassen E, Jensen JS, Sigmund O. On the realization of the bulk modulus bounds for two-phase viscoelastic composites. Journal of the Mechanics and Physics of Solids. 2014;63:228-41.

32. Yi Y-M, Park S-H, Youn S-K. Design of microstructures of viscoelastic composites for optimal damping characteristics. International Journal of Solids and Structures. 2000;37(35):4791-810.

33. Sanchez-Palencia E. Non-Homogenous Media and Vibration Theory. Lecture Notes in Physics. 1980;127(127).

34. Papanicolau G, Bensoussan A, Lions J-L. Asymptotic analysis for periodic structures: Elsevier; 1978.

35. Kohn RV, Vogelius M. A new model for thin plates with rapidly varying thickness. International Journal of Solids and Structures. 1984;20(4):333-50.

36. Kalamkarov A. On the determination of effective characteristics of cellular plates and shells of periodic structure. Mech Solids. 1987;22(2):175-9.

37. Saha GC, Kalamkarov AL, Georgiades AV. Asymptotic homogenization modeling and analysis of effective properties of smart composite reinforced and sandwich shells. International Journal of Mechanical Sciences. 2007;49(2):138-50.

38. Kalamkarov AL, Hassan EM, Georgiades A, Savi M. Asymptotic homogenization model for 3D grid-reinforced composite structures with generally orthotropic reinforcements. Composite structures. 2009;89(2):186-96.

39. Adam L, Depouhon A, Assaker R. Multi-scale modeling of crash & failure of reinforced plastics parts with digimat to ls-dyna interface. 7th European LS-DYNA Conference; 2009.

40. Landervik M, Jergeus J. Digimat Material Model for Short Fiber Reinforced Plastics at Volvo Car Corporation. European LS-DYNA Conference; 2015.

41. Yuan Z, Crouch R, Wollschlager J, Fish J. Assessment of multiscale designer for fatigue life prediction of advanced composite aircraft structures. 2017;51(15):2131-41.

42. Yu W, Liu X. SwiftComp. 2017. https://cdmhub.org/resources/scstandard.

43. MacKrell A. Multiscale composite analysis in Abaqus: Theory and motivations. Reinforced Plastics. 2017;61(3):153-6.

44. Cheng GD, Cai YW, Xu L. Novel implementation of homogenization method to predict

effective properties of periodic materials. Acta Mechanica Sinica. 2013;29(4):550-6.

45. Cai Y, Xu L, Cheng G. Novel numerical implementation of asymptotic homogenization method for periodic plate structures. International Journal of Solids & Structures. 2014;51(1):284–92.

46. Wang B, Tian K, Hao P, Cai Y, Li Y, Sun Y. Hybrid analysis and optimization of hierarchical stiffened plates based on asymptotic homogenization method. Composite Structures. 2015;132:136-47.

47. Xu L, Cheng G. Shear stiffness prediction of Reissner-Mindlin plates with periodic microstructures. Mechanics of Advanced Materials and Structures. 2016(just-accepted).

48. Xu L, Yi GC, Sinan. A New Method of Shear Stiffness Prediction of Periodic Timoshenko Beams. Mechanics of Advanced Materials & Structures. 2015:00-.

49. Yi S, Xu L, Cheng G, Cai Y. FEM formulation of homogenization method for effective properties of periodic heterogeneous beam and size effect of basic cell in thickness direction. Computers & Structures. 2015;156:1-11.

50. Zhang Y, Shang S, Liu S. A novel implementation algorithm of asymptotic homogenization for predicting the effective coefficient of thermal expansion of periodic composite materials. Acta Mechanica Sinica. 2017:1-14.

51. Zhao J, Li H, Cheng G, Cai Y. On predicting the effective elastic properties of polymer nanocomposites by novel numerical implementation of asymptotic homogenization method. Composite Structures. 2016;135:297-305.

52. Kalamkarov AL, Andrianov IV, Danishevs'kyy VV. Asymptotic Homogenization of Composite Materials and Structures. Applied Mechanics Reviews. 2009;62(3):030802-.

53. Christensen RM, Freund LB. Theory of viscoelasticity. Journal of Applied Mechanics. 2003;38(3):720.

54. Parnell WJ, Abrahams ID. Dynamic homogenization in periodic fibre reinforced media. Quasi-static limit for SH waves. Wave Motion. 2006;43(6):474-98.

55. Parnell WJ, Abrahams ID. Homogenization for wave propagation in periodic fibre-reinforced media with complex microstructure. I—Theory. Journal of the Mechanics and Physics of Solids. 2008;56(7):2521-40.

56. Sigmund O. Materials with prescribed constitutive parameters: an inverse homogenization problem. International Journal of Solids and Structures. 1994;31(17):2313-29.

57. Liu S, Cheng G, Gu Y, Zheng X. Mapping method for sensitivity analysis of composite material property. Structural and multidisciplinary optimization. 2002;24(3):212-7.

58. Deshpande VS, Fleck NA, Ashby MF. Effective properties of the octet-truss lattice material. Journal of the Mechanics and Physics of Solids. 2001;49(8):1747-69.